sustainability

MDPI

Article

Harmonics Minimisation in Non-Linear Grid System Using an Intelligent Hysteresis Current Controller Operated from a Solar Powered ZETA Converter

Lakshmana Perumal Pattathurani [1,*], Subhransu S. Dash [2], Rajat K. Dwibedi [3], Mani Devesh Raj [4], Raju Kannadasan [5], Max F. Savio [6], Mohammed H. Alsharif [7] and James Hyungkwan Kim [8,*]

1 Faculty of Electrical Engineering, Sathyabama Institute of Science and Technology, Chennai 600119, Tamil Nadu, India
2 Department of Electrical Engineering, Government College of Engineering, Keonjhar 758002, Odisha, India; munu_dash_2k@yahoo.com
3 Department of Electronics and Communication Engineering, Aarupadai Veedu Institute of Technology, Chennai 603104, Tamil Nadu, India; rajatsrr@gmail.com
4 Department of Electrical and Electronics Engineering, Sri Sivasubramaniya Nadar College of Engineering, Kalavakkam 603110, Tamil Nadu, India; deveshrajm@ssn.edu.in
5 Department of Electrical and Electronics Engineering, Sri Venkateswara College of Engineering, Kanchipuram 602117, Tamil Nadu, India; kannan.3333@yahoo.co.in
6 Department of Electrical and Electronics Engineering, Saveetha Engineering College, Chennai 602105, Tamil Nadu, India; maxsaviofrancis@gmail.com
7 Department of Electrical Engineering, College of Electronics and Information Engineering, Sejong University, Seoul 05006, Korea; malsharif@sejong.ac.kr
8 Lawrence Berkeley National Laboratory, 1 Cyclotron Road, Berkeley, CA 94720, USA
* Correspondence: ranipattathu670@gmail.com (L.P.P.); hyungkwankim@lbl.gov (J.H.K.)

Citation: Pattathurani, L.P.; Dash, S.S.; Dwibedi, R.K.; Raj, M.D.; Kannadasan, R.; Savio, M.F.; Alsharif, M.H.; Kim, J.H. Harmonics Minimisation in Non-Linear Grid System Using an Intelligent Hysteresis Current Controller Operated from a Solar Powered ZETA Converter. *Sustainability* **2022**, *14*, 7028. https://doi.org/10.3390/su14127028

Academic Editor: José Luis Domínguez-García

Received: 26 April 2022
Accepted: 7 June 2022
Published: 8 June 2022

Abstract: Due to the non-linear load characteristics in the domestic three-phase grid system, the quality of power transmission is a challenge for researchers. In this paper, the harmonics injected in a three-phase grid system due to the non-linear loads and a solution for harmonics minimisation using the hysteresis current controller (HCC) is presented. The proposed work consists of switched dc loads such as personal computers, SMPS, etc., connected to the three-phase grid system through the rectifier unit. These loads connected with other AC loads inject harmonics in the power lines. The total harmonic distortion (THD) at the power line is therefore increased. A ZETA embedded three-phase inverter using an artificial neural network-based HCC (ANN-HCC) is used to minimise the voltage and the current THDs. To ease the power consumption, a solar photovoltaic system (SPV) is used to power the ZETA embedded three-phase inverter. The output of the SPV is regulated using the ZETA dc/dc converter. However, the hysteresis bands (U_{upper} and U_{lower}) are selected using the ANN with respect to the actual value compared with the calculated current error. The vector shifts to the next based on the previous vector applied, and thereby the process repeats following the same pattern. The back propagation (BP)-based neural network is trained using the currents' non-linear and differential functions to generate the current error. The neural structure ends when the value hits the hysteresis band. Simultaneously, the PWM control waveform is tracked by the neural network output. The proposed system is mathematically modelled using MATLAB/Simulink. An experimental setup of a similar prototype model is designed. The voltage and the current harmonics are measured using a Yokogawa CW240 power quality meter and the results are discussed.

Keywords: artificial neural network (ANN); solar photovoltaic; switch-mode power supply; power quality; total harmonic distortions; hysteresis current controller; ZETA converter

1. Introduction

Distributed generations (DGs) have become a striking choice for integrating power distribution systems due to their cost-effective, technical, and ecological benefits [1–3].

Additionally, the advancement in the three-phase power distribution system has introduced the dc/dc converters for their contribution to the power quality improvements. The power quality parameters such as active power flow direction, reactive power, harmonics, and power factor play an essential role in the grid power system [4]. In recent studies, non-linear loads are more commonly found and produce disturbances to other loads in the grid systems that are weak or remote systems. Consequently, the grid connecting both three-phase and single-phase domestic or residential appliances is affected due to the injection of current harmonics in the line, which lowers the power quality of the overall system. The total harmonic distortion (THD) is a series of issues emerging from the non-linear loads connected in the grid system.

The origin of the power system harmonics is due to the characteristic behaviour of the non-linear loads such as uninterrupted power supply (UPS), TVs, computers, printers, adjustable speed drives, fluorescent lighting, arc furnaces, and transformers [5]. These non-linear devices used in residential homes generate current harmonics injected into the grid system that affect other loads. These non-linear distorted waves are identical to the 3rd, 5th, and 7th harmonics that are referred to as the harmonic impedances associated with the current harmonics [6]. The harmonics sources at the point of common coupling are planned with harmonic distortion limits, quality of electric supply, equipment performances, and utilities [7]. When non-linear loads are connected in the distribution system, the performance of the system deviates outside the desired standard value. Hence, the harmonics are to be monitored in the distribution system involving non-linear loads. The harmonics monitoring management is carried out based on the international and national standards [8,9]. The current and voltage harmonic distortions have different standards to maintain depending on the type of load. However, most loads need to have lower current harmonics and within limits during operation.

Several works reported the effectiveness of the converting techniques and their controllers adapted for power quality improvement using sophisticated approaches. Authors also proposed a model predictive control (MPC) method for microgrids that maintains the power quality by regulating the converters to attain the required criteria [10]. These approaches are adopted successfully for interconnected and islanded systems. Further, to overcome the power quality degradation, artificial neural networks (ANNs) and hybrid differential evolution (HDE) are involved in reinstating the frequency and voltage considering the disturbances [11]. Some works proposed a chopper, two PI controllers, and an inverter to improve a fuel cell's power quality interconnected with the power system network [12]. Each PI controller was tuned using three different evolutionary programs: electromagnetic field optimisation (EFO), modified flower pollination algorithm (MFPA), and harmony search (HS).

Moreover, a unique ANN-based control method that minimized the sag, swell, unbalancing, voltage deviation, frequency, and THD was demonstrated [13]. Further, some researchers recommended a shunt active power filter (SAPF) for microgrid systems encompassing solar, wind, and fuel cell-based distributed generation, and the influence of power quality hitches in an adopted standalone was explored [14]. An upgraded custom power device, namely a distributed power condition controller, was adapted to a multi-microgrid system with greater penetration of various distributed generators on the island and interconnected modes to increase the power quality [15]. An optimal control mechanism for a multi-level converter [16,17] was developed, and this control scheme alleviated the glitches caused by the conventional approaches. Authors also reported a solution to resolve the fast dynamic concerns and fixed-frequency operation using a whole, robust voltage control scheme and angle droop approaches [18]. It is also reported as a robust, fast, and dynamic PI resonance controller with a harmonic compensator (HC) and lead compensator (LC) feedback to manage the current of a 15-level neutral-point-clamped multi-level inverter [19]. In addition, a unified power quality conditioner was suggested as a consistent power quality conditioner for a nine-level structure [20].

Moreover, the most common concern is the accuracy of the harmonic measurements due to their complexity in design, so they are challenging to implement. Furthermore, the measure based on the active power flow, reactive power, and current–voltage ratio is still not accurate; each method has advantages and disadvantages. Various non-linear controllers are available that monitor and control the voltage and current harmonics in the three-phase line. Predictive control (PC), hysteresis current controller (HCC), and sliding mode controllers (SMCs) have been developed by researchers. Among the current controllers, the hysteresis current controller [21] (HCC) is most preferred for its simple design, fast response, and strong robustness to disturbances. However, a space vector-based hysteresis current controller [22,23] is designed for a fast response. In this method, the stator voltages along α and β axes are estimated using current error information and the steady state model of the induction machine. Consistently, the steady-state boundaries and the phase voltages are normalised, and the switching frequency is maintained constant.

Moreover, the zero-sequence current can be suppressed using a wide linear modulation range of zero-sequence voltage-based SVPWM [23]. This is performed by controlling the fundamental plane. The harmonics' source can be estimated using key factors such as current cancellation due to phase angle diversity and the attenuation owing to system impedance. Certain digital controllers such as analogue-to-digital converters produce variable hysteresis controller bands that are insufficient to stabilise. A digital hysteresis current controller uses a mixed-level scheme [24,25] and prediction-based sampling method to estimate the switching frequency variations in the grid voltage and resolve the switching frequency, respectively. This provides greater comfort for the digital hysteresis current controller, ensuring stabilised switching frequency and high-quality grid-side filtered current.

In modern technology, the DC/DC converter plays a vital role in the dc micro-grid system. The non-linear load present is controlled by the dc/dc converters that provide non-linear bifurcation phenomena for the complex design. The analogue hysteresis controller exploits the oversampling [26], and DC to DC converters are used. Among the dc/dc converters, ZETA converters [27–29] are more efficient in operating in continuous conduction mode. Moreover, the converter can work both in buck and boost operation. ZETA converters have very low current harmonics and are usually preferred for drive applications. The proposed system thereby uses a power quality enhancement based on a ZETA converter for the PWM-based three-phase inverter. The current ripple is reduced and helps the inverter circuit regulate the bandwidth range of the hysteresis current controller. The variable band control of the HCC can be performed more efficiently by the intelligent controllers. The artificial neural network-based hysteresis current controller [30,31] has resulted in lower switching losses of the inverter and the ability to control the frequency constantly. Additionally, the bandwidth approaches the reference value to obtain the reduced THDs.

From the above literature survey, it is seen that the behaviour of the non-linear loads such as uninterrupted power supply (UPS), TVs, computers, printers, adjustable speed drives, fluorescent lighting, arc furnaces, and transformers causes the injection of harmonics into the grid system. This affects the overall performance. The proposed method deals with the modelling of the ANN-based HCC for the grid system.

2. Proposed Model

Since the globally increasing modernisation of infrastructure is one of the driving factors leading to the demand for electric power generation, the proposed system uses the solar photovoltaic system to power the dc/dc converter (Figure 1). The ZETA converter is used as the MPPT converter [32] for the solar PV. As discussed, the ZETA converter is in the buck–boost converter family, and a boundless region for maximum power point tracking (MPPT) is achieved. The proposed three-phase grid system has non-linear loads connected in parallel along with other loads. The voltage and the current harmonics injected into the three-phase grid voltages are analysed, and an intelligent controlled ZETA-based hysteresis current controller is proposed.

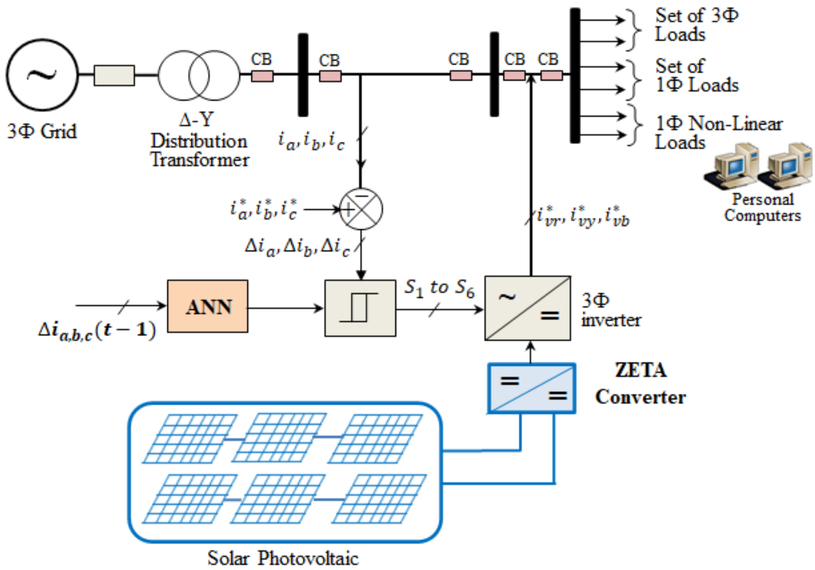

Figure 1. Design of proposed renewable energy distributed generation system.

The proposed system involves the renewable energy distributed generation (REDG) system connected to a three-phase, four-leg inverter injecting the power back into the three-phase grid. The three-phase grid system is powering the sets of three-phase and single-phase loads. Multiple units of personal computers (SMPS loads) are connected along with other loads. We have considered this commercial utility as being primarily powered by a three-phase line through a delta-to-star-connected distribution transformer. The three-phase grid system is thus obtained for utility purposes. The modelling of the proposed system is described in the following sections.

2.1. Modelling of the Solar PV

The ZETA embedded three-phase inverter is powered using the solar photovoltaic system. The size of the solar PV is slightly larger than the magnitude of the grid voltage in consideration of the losses. Hence, a solar maximum peak power, P_{mpp} = 3.4 kW, is well sufficient to power slightly above the peak voltage in the three-phase grid. Vikram 280 W polycrystalline solar panels are selected for the SPV array of an appropriate size. The solar power, P_m = 280 W, open circuit voltage, V_{oc} = 38.70 V, voltage at maximum power, V_m = 31.3 V, short-circuit current, I_{sc} = 9.32 A, current at maximum power, I_m = 8.94 A, are the specifications of the solar panel selected.

2.2. Modelling of ZETA Embedded Three-Phase Inverter

The ZETA dc/dc converter is capable of operating both in the buck and the boost mode by adjusting the duty ratio. Moreover, the efficiency and the voltage gain are better than a regular buck–boost converter. The ZETA embedded three phase inverter is the combination of the ZETA converter with a two-level inverter. In power flow between the AC grid and renewable energy systems (RESs) or any intermittent DC voltage levels, the intermediate circuit capacitor (dc-link) plays a vital role. Due to the variable nature of RESs, the variation in the current is subjected to peak values irregularly. An intermediate circuit capacitor of high value with the ability to withstand these variations and supply sufficient power is required. A typical ZETA converter with the dc-link capacitors is designed to have high values, which may be superimposed with high-frequency ripple voltages of 500 VDC to 1500 VDC. Figure 2 shows the ZETA embedded three-phase inverter.

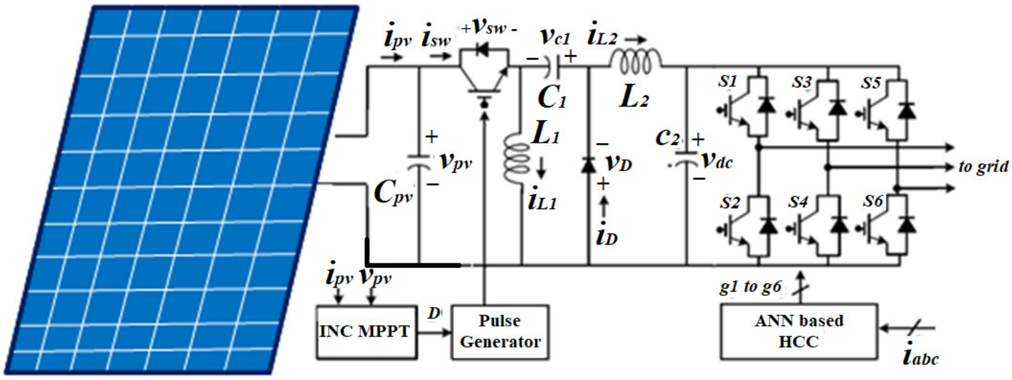

Figure 2. ZETA embedded 3Φ inverter.

The ZETA converter is a highly efficient converter operating in buck and boost mode. The output of the ZETA converter is responsible for the voltage across the dc-link. The components of the ZETA converter are designed to always operate in the continuous conduction mode (CCM). The design consists of input and the output inductors (L_1 and L_2) with an intermediate capacitor (C_1). The design of the ZETA converter is estimated from the duty cycle (δ).

$$\text{Duty Cycle, } \delta = \frac{V_{dc}}{V_{dc} + V_{mpp}} \tag{1}$$

where V_{dc} is an average value of the ZETA output voltage and V_{mpp} is the maximum peak to peak voltage of the solar panel. Under standard test conditions (STCs), for the given model of the solar panel, V_{mpp} = 287.20 V and I_{mpp} = 11.83 A.

For V_{dc} = 300 V, the duty cycle from the Equation (1) is obtained as

$$\delta = \frac{300}{300 + 287.20} = 0.51. \tag{2}$$

Let I_{dc} be the average current that flows through the dc-link of the VSI. It is estimated as

$$I_{dc} = \frac{P_{mpp}}{V_{dc}} = \frac{3400}{300} = 11.33 \text{ A}. \tag{3}$$

The value of the inductors (L_1, L_2) and capacitor (C_1) is estimated as

$$L_1 = \frac{\delta V_{mpp}}{f_{sw} \Delta I_{L1}} = \frac{0.62 * 287.20}{20000 * 11.83 * 0.06} = 10 \text{ mH}, \tag{4}$$

$$L_2 = \frac{(1-\delta) V_{mpp}}{f_{sw} \Delta I_{L2}} = \frac{(1-0.62) * 287.20}{20000 * 11.33 * 0.06} = 10 \text{ mH}, \tag{5}$$

$$C_1 = \frac{\delta I_{dc}}{f_{sw} \Delta I_{C2}} = \frac{(0.51) * 11.33}{20000 * 300 * 0.1} = 9.6\ \mu\text{F}. \tag{6}$$

2.3. ANN-Based HCC Model

The modelling of the hysteresis current controller (HCC) is done using the current vector components of the three-phase system. Consider a three-phase inverter with six switches. The switches are switched in complementary order such that no two switches in a single leg are turned ON at the same time. The pulse generated for each switch is restricted to turn ON the switches of the same leg. The HCC practically compares the current in each leg with the reference value. The HCC is designed to generate a hysteresis band (U_{upper} and U_{lower}). When the phase current exceeds the reference current, the lower switch is closed and, when it falls short, the upper switch is closed.

The d-axis reference current is set to zero $\left(i_d^*\right)$. According to the Park's transformation, i_d^*, i_q^*, and the phase angle φ_e are transferred to the reference phase currents $\left(i_{abc}^*\right) = \left[i_a^*, i_b^*, i_c^*\right]$. The matrix representation is given as

$$\begin{bmatrix} i_a^* \\ i_b^* \\ i_c^* \end{bmatrix} = \begin{bmatrix} \cos(\varphi_e) & \sin(-\varphi_e) \\ \cos(\varphi_e - 120^o) & \sin(120^o - \varphi_e) \\ \cos(\varphi_e - 240^o) & \sin(120^o - \varphi_e) \end{bmatrix} \begin{bmatrix} i_d^* \\ i_q^* \end{bmatrix}. \quad (7)$$

The third phase current can be obtained from the measured phase currents i_A and i_B and is given as

$$i_c = -(i_a + i_b). \quad (8)$$

The reference current i_{abc}^* and the phase currents i_{abc} are compared with the hysteresis comparator. The novel hysteresis current controller uses an artificial neural network to obtain the switching states of phase A, B, and C. The switching states are represented as $k_{abc} = [k_a, k_b, k_c]$. At each stage of the switching, the back propogation methodology finds the minimum value of the error function in weighted space. On obtaining the minimum error function, the value of the switching states is fixed using the below equations:

$$k_p = \begin{cases} 1, \ \Delta i_p > +H \\ 0, \ \Delta i_p < -H \end{cases} \quad (9)$$

where Δi_p is the phase current error, H is the hysteresis band. The band limit is obtained as $U_{upper} = +H$ and $U_{lower} = -H$. The phase switching state k_p is unchanged when the current error Δi_p is well defined within the limit. Thus, the current distortions are controlled within the limit. Figure 3 shows the hysteresis band across the measured current traced with a bandwidth of 2 H (i.e., $BW = +H - (-H)$). The point P_2 is found to be within the range, hence the value of k_p is freely implemented. This region is called the free region. For the point P_1, the value outside the range (unfree region) has to be enforced to bring the point within the range so as to satisfy Equation (9).

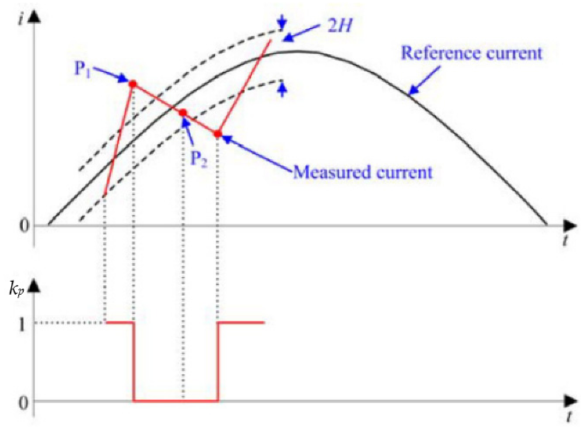

Figure 3. Representation of HCC in current waveforms (i_p denotes the pulse current).

The ANN-based hysteresis current controller (ANN–HCC) is shown in Figure 4. The ANN is applied through the PMW mechanism to regulate the grid current. By setting the amplitude of the triangular waveform to 1, the ratio of the output current to the ANN output is determined. This is the gain of the PWM that must equal the current error Δi_p, approximately close to zero. For the points occurring outside the free region, the approximation is calculated from the state space model.

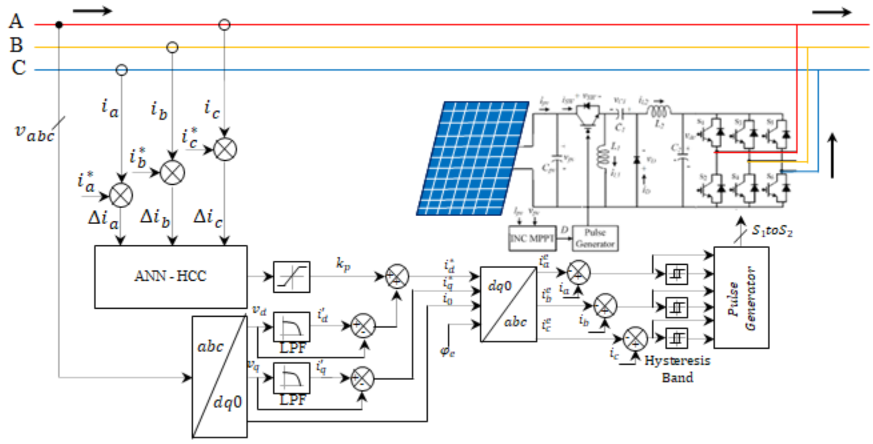

Figure 4. Modelling of ANN-based hysteresis current controller.

The ANN controls the band limit and enforces the points that are away from the free region. The ANN is trained to minimise the time taken to bring the point outside the free region. By using the back propagation algorithm, the initial switching states are set with respect to the weight vector of the three-phase current.

The back propagation functions in two steps. The first step is to set the initial switching state of the current vector. The value of k_p is set such that the band (U_{lower} and U_{upper}) is within the range.

The time required for the training typically depends on the amount of the training data. The determination of network size involves conciliation between output accuracy, preparation time, and ANN speculation capacities. There is no broad methodology for deciding the right ANN size for a particular issue. The nested loop structure has a slower outer loop formed by the faster inner loop—the three-layered feed-forward NN and the four-layered feed-backward NN form the back propagation technique. The proposed ANN consists of 3 hidden layers of 6 nodes each (Figure 5).

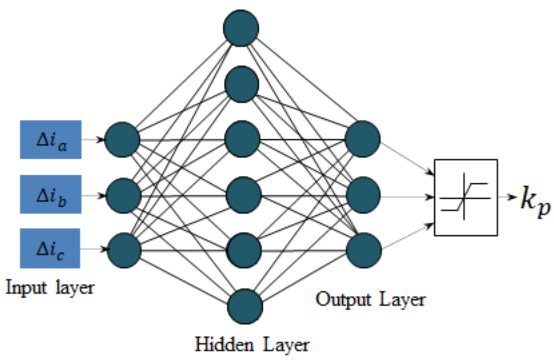

Figure 5. Arrangement of artificial neural network.

3. Simulation Results

The proposed three-phase solar interfaced grid system is initially verified mathematically using MATLAB/Simulink. The grid system powers various sets of loads. The solar output is inverted using a four-leg inverter and back supplied to the three-phase grid. The dc-link voltage is found to be constant throughout the work. The set of non-linear SMPS loads measures the load voltage and the current. The harmonics injected into the three-phase grid are measured. The system is thereby modelled with a closed-loop ANN-HCC to verify the harmonic levels. The waveforms of the input side grid voltages (V_r, V_y, V_b), input side grid currents (I_r, I_y, I_b), load side grid currents (I_{lr}, I_{ly}, I_{lb}), inverter currents (I_{r_inv}, I_{y_inv}, I_{b_inv}), and dc-link voltages are shown in Figure 6.

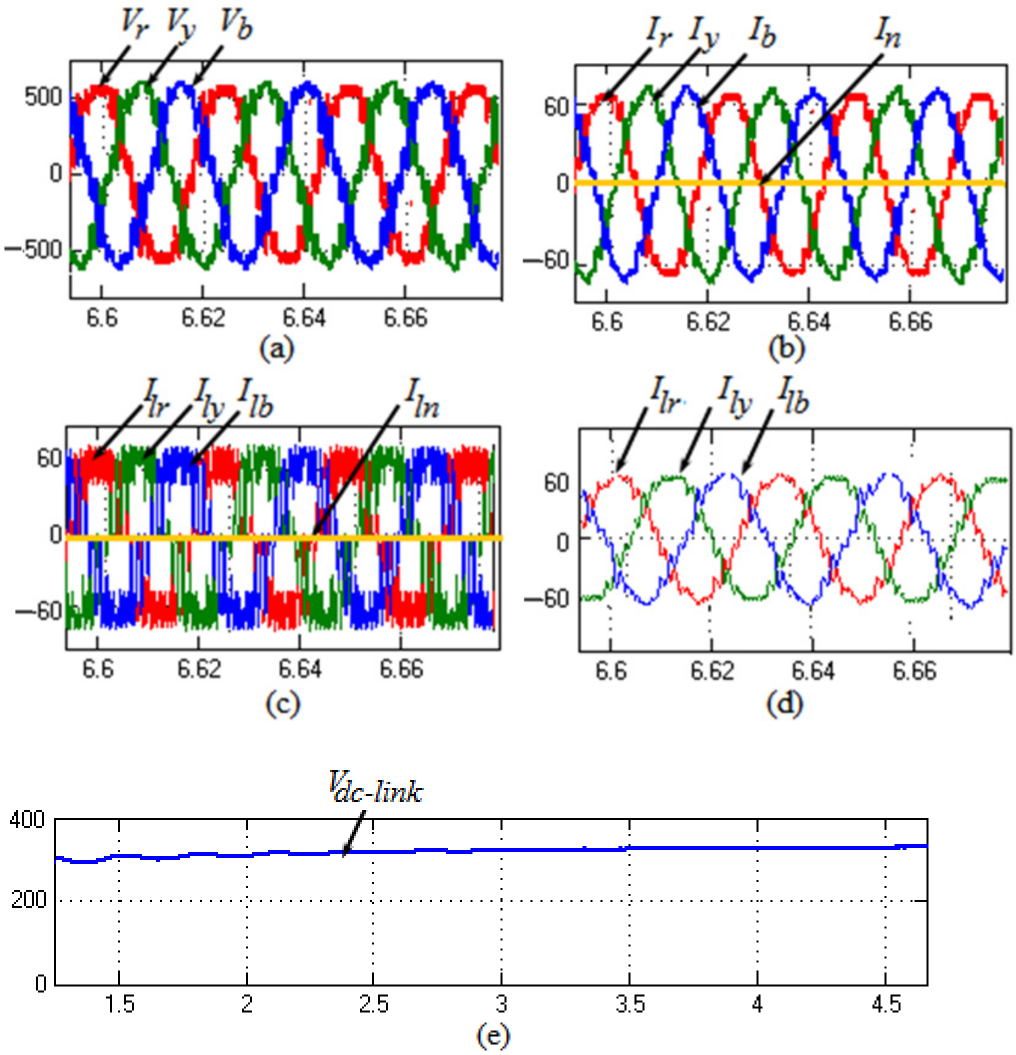

Figure 6. Simulation results: (**a**) grid voltage at input side, (**b**) grid current at input side, (**c**) grid current at output side before HCC, (**d**) grid current at output side after HCC inverter current, and (**e**) dc-link voltage.

The peak significance of grid current and voltages at the input side is measured as I_{peak} = 60 A and V_{peak} = 500 V, respectively (Figure 6a,b). The system is connected to the non-linear load that injects the harmonics into the grid. The load side peak value of grid current is I_{load} = 60 A (Figure 6c). The inverter current obtained from the solar interfacing is injected back into the grid. The inverter current was measured as I_{inv} = 15 A (Figure 6d). The dc-link capacitor is designed to produce a voltage of about V_{dc} = 300 V (Figure 6e).

The single phase obtained from the phase-neutral of the three-phase connection is modelled as the single-phase connection is connected to the non-linear SMPS loads and the rectifier units forming a set of non-linear loads connected to it. The phase voltage and the currents of the single-phase system are measured to have the phase peak values of I_{ph} = 30 A, V_{ph} = 300 V, respectively (Figure 7a,b).

Figure 8 shows the harmonics obtained through the FFT analysis in MATLAB/Simulink. At the fundamental frequency of 50Hz, the magnitude of the total harmonic distortions (THD) with respect to the fundamental value is noted. The voltage and the current harmonics are measured with and without the HCC. The voltage and current THD without the HCC are measured as 27.62% and 7.52%, respectively (Figure 8a,b). The voltage and the current THD with the HCC are measured as 17.62% and 2.56%, respectively (Figure 8c,d).

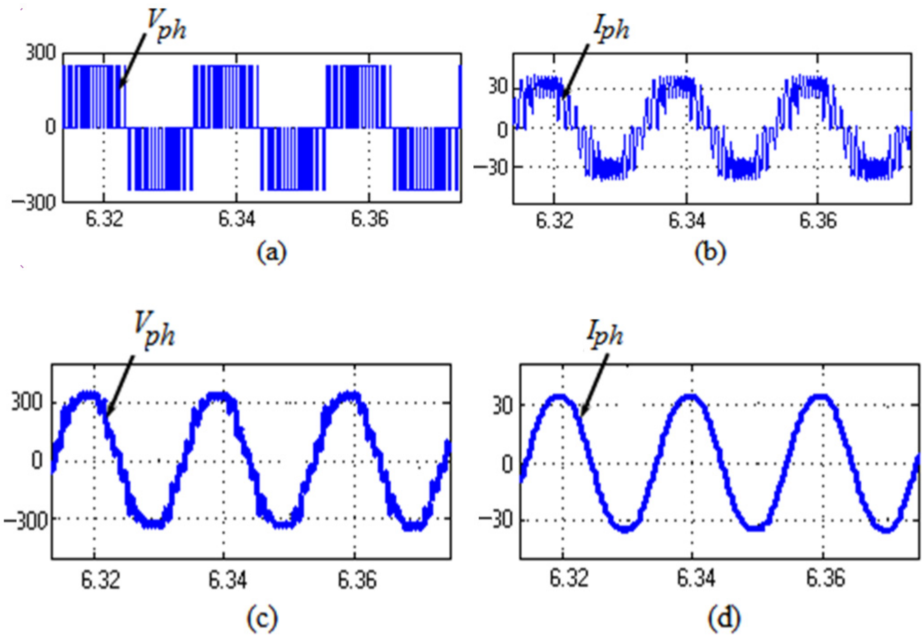

Figure 7. Simulation results: 1Φ load terminal (**a**) voltage waveform before HCC, (**b**) current waveform before HCC, (**c**) voltage waveform after HCC, and (**d**) current waveform after HCC.

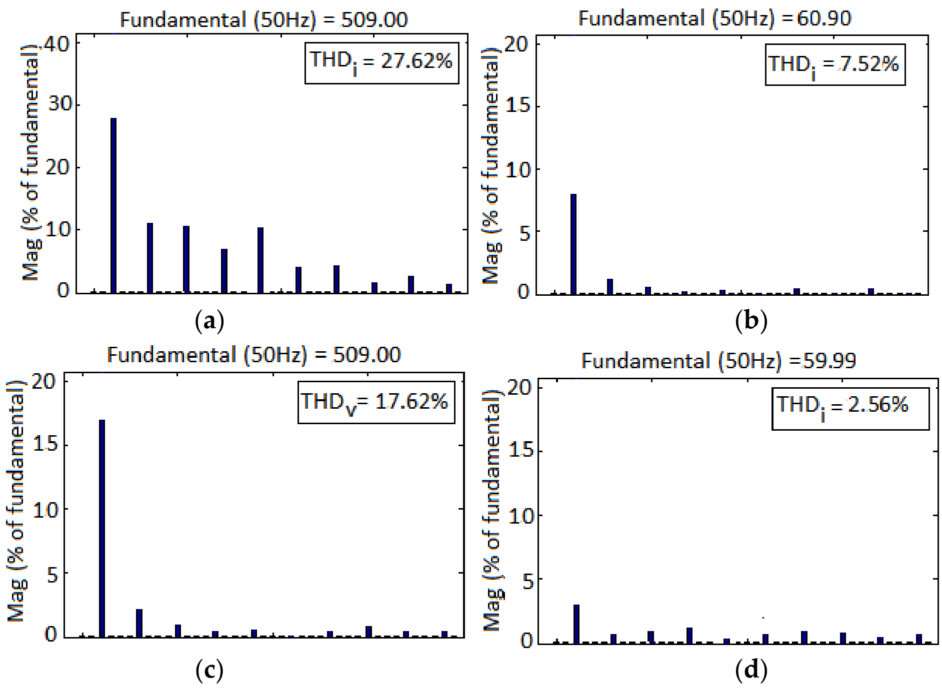

Figure 8. Total harmonic distortions: (**a**) voltage THD with HCC, (**b**) current THD without HCC, (**c**) voltage THD with HCC, (**d**) current THD with HCC.

4. Experimental Validation

The experiment is validated using a single-phase line taken from the three-phase, 4 W distribution system. The experiment is tested for the single-phase line feeding the non-linear loads for convenience. The system considerations are tabulated in Table 1.

Table 1. Experimental system parameters.

Three-phase supply (r.m.s):	$V_{l\text{-}l}$ = 400 V, 50 Hz
Single-phase supply (r.m.s):	V_{ph} = 230 V, 50 Hz
Single-phase linear load:	R = 36.66 Ω, L = 10 mH
Single-phase non-linear load:	R = 26.66 Ω, L = 10 mH
dc-link parameters:	C = 3000 µF, V_{dc} = 120 V

Using the three-phase voltage source inverter, the dc-link voltage has been inverted. Figure 9a shows the three-phase input voltage of 664 V. The three-phase input current of 40 A is shown in Figure 9b. The proposed system output current of 20 A is shown in Figure 9c, and the dc-link is measured as V_{dc} = 120 V and shown in Figure 9d.

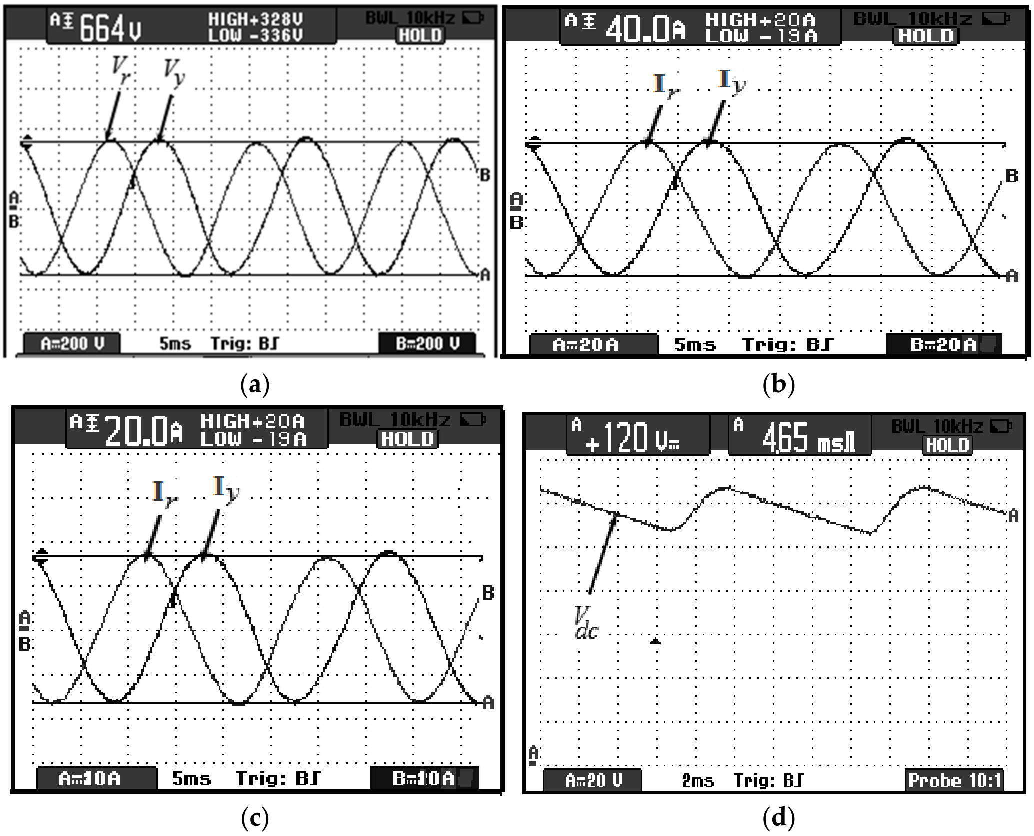

Figure 9. Experimental results: (**a**) input side voltage, (**b**) input side current, (**c**) current output, (**d**) dc-link voltage.

The total harmonic distortions are measured for the proposed system. The THD measured for the voltage and current without and with the HCC is shown in Figure 10. The voltage and current THDs measured without the HCC are shown in Figure 10a,b. The voltage THD without the HCC is 30.80%, and the current THDs without the HCC are 14.10%. The HCC is designed, and the THDs of voltage and current are noted. Figure 10c,d show the voltage and the current THDs measured with the HCC. The voltage THD using the HCC is found to be 10.60%, and the current THD using the HCC is found to be 2.50%.

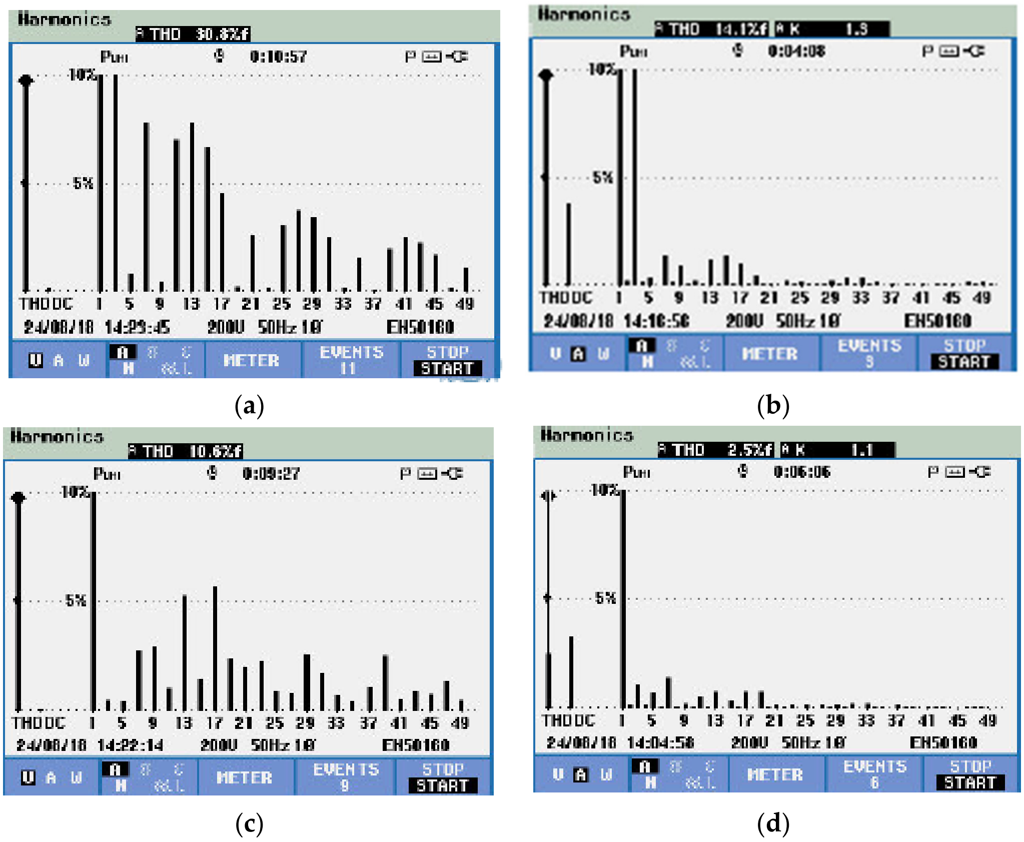

Figure 10. Experimental THDs: (**a**) voltage without HCC, (**b**) current without HCC, (**c**) voltage with HCC, (**d**) current with HCC.

5. Comparative Analysis

To study the reliability of the proposed model, THD values are compared between the simulation and hardware experimentation with the HCC and without the HCC in Figures 11 and 12.

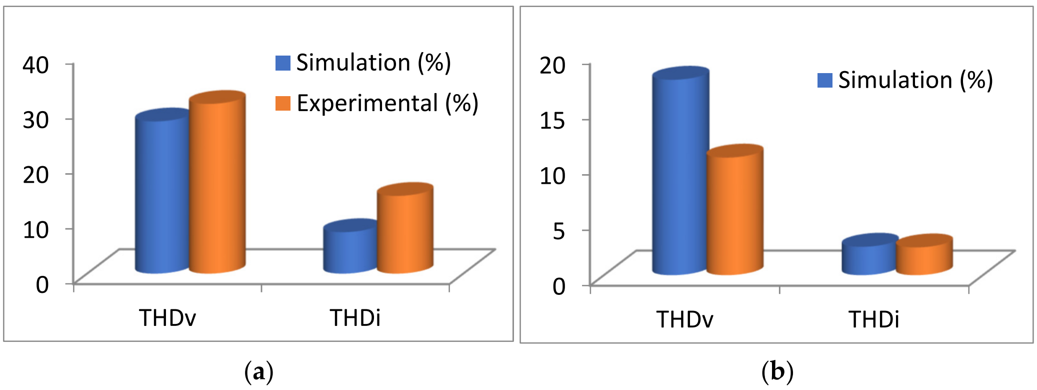

Figure 11. Comparative analyses between simulated and experimental results: (**a**) simulated results, (**b**) experimental results.

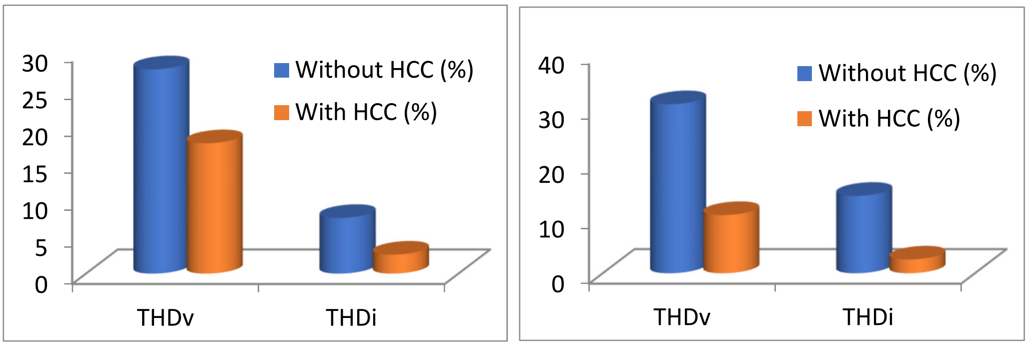

(**a**) (**b**)

Figure 12. Comparative analyses between two cases (with and without HCC and ANN): (**a**) simulated results, (**b**) experimental results.

The above figures compare the total harmonic distortion (THD) of the current and the voltage obtained with and without the HCC. This analysis indicates that the experimental and simulated results are relatively close for both voltage and current THD. Further, the HCC controlled using the artificial neural network is more efficient with a reduced THD scale, with simulated voltage and current THDs of 17.62% and 2.56%, respectively, and experimental voltage and current THDs of 10.60% and 2.50%, respectively.

6. Conclusions

The proposed system is mathematically modelled using an advanced converting technique along with an ANN, and the research was carried out to study the harmonic distortion in the non-linear loads. The special computers are considered to be the non-linear loads, and the proposed mathematical modelling is performed for a more extensive system of AC grid voltage of 1100 V. The current and the voltage THDs are calculated, and it is observed that the system without the hysteresis current controller (HCC) develops high THD values of voltage and current. The HCC is used for a similar system using an ANN and offers reduced voltage and current THDs. However, the ANN plays a vital role, the THD levels are well reduced, and the power quality is improved for the non-linear system. Compared with the conventional approach, the ANN-based hysteresis current controller has diminished both the voltage and the current THDs to 10.60% and 2.50%, respectively. Moreover, the ZETA converter control on the dc-link is more efficient for the HCC to control the non-linear loads in the three-phase grid system feeding various types of loads. This proposed system can be effectively used for the power quality improvement of the renewable-based distribution system.

Author Contributions: Conceptualization, L.P.P.; Formal analysis, S.S.D. and J.H.K.; Funding acquisition, J.H.K.; Investigation, S.S.D., R.K.D., M.D.R., M.H.A. and J.H.K.; Methodology, R.K.D. and R.K.; Project administration, R.K. and M.H.A.; Resources, M.F.S.; Software, L.P.P. and M.F.S.; Supervision, M.D.R.; Validation, M.H.A.; Writing—original draft, L.P.P., R.K. and M.F.S.; Writing—review & editing, M.D.R. and J.H.K. All authors have read and agreed to the published version of the manuscript.

Funding: This study was supported by the Hewlett Foundation.

Institutional Review Board Statement: Not applicable.

Informed Consent Statement: Not applicable.

Data Availability Statement: Not applicable.

Conflicts of Interest: The authors declare no conflict of interest.

References

1. Venkatesan, C.; Kannadasan, R.; Alsharif, M.; Kim, M.-K.; Nebhen, J. Assessment and Integration of Renewable Energy Resources Installations with Reactive Power Compensator in Indian Utility Power System Network. *Electronics* **2021**, *10*, 912. [CrossRef]
2. Venkatesan, C.; Kannadasan, R.; Alsharif, M.; Kim, M.-K.; Nebhen, J. A Novel Multiobjective Hybrid Technique for Siting and Sizing of Distributed Generation and Capacitor Banks in Radial Distribution Systems. *Sustainability* **2021**, *13*, 3308. [CrossRef]
3. Venkatesan, C.; Kannadasan, R.; Ravikumar, D.; Loganathan, V.; Alsharif, M.H.; Choi, D.; Hong, J.; Geem, Z.W. Re-Allocation of Distributed Generations Using Available Renewable Potential Based Multi-Criterion-Multi-Objective Hybrid Technique. *Sustainability* **2021**, *13*, 13709. [CrossRef]
4. Rajalakshmi, M.; Chandramohan, S.; Kannadasan, R.; Alsharif, M.; Kim, M.-K.; Nebhen, J. Design and Validation of BAT Algorithm-Based Photovoltaic System Using Simplified High Gain Quasi Boost Inverter. *Energies* **2021**, *14*, 1086. [CrossRef]
5. Vora, S.; Bhatt, D. A Comprehensive Review of Harmonics Effects on Electrical Power Quality. *Int. J. Eng. Dev. Res.* **2014**, *1*, 15–21.
6. Du, Q.; Gao, L.; Li, Q.; Li, T.; Meng, F. Harmonic Reduction Methods at D.C. Side of Parallel-Connected Multipulse Rectifiers: A Review. *IEEE Trans. Power Electron.* **2021**, *36*, 2768–2782.
7. Hintz, A.; Prasanna, U.R.; Rajashekara, K. Comparative Study of the Three-Phase Grid-Connected Inverter Sharing Unbalanced Three-Phase and/or Single-Phase systems. *IEEE Trans. Ind. Appl.* **2016**, *52*, 5156–5164. [CrossRef]
8. Sinvula, R.; Abo-Al-Ez, K.M.; Kahn, M.T.E. Harmonic Source Detection Methods: A Systematic Literature Review. *IEEE Access* **2019**, *7*, 74283–74299. [CrossRef]
9. McBee, K.D.; Simoes, M. Evaluating the Long-Term Impact of a Continuously Increasing Harmonic Demand on Feeder-Level Voltage Distortion. *IEEE Trans. Ind. Appl.* **2013**, *50*, 2142–2149. [CrossRef]
10. Garcia-Torres, F.; Vazquez, S.; Moreno-Garcia, I.; Gil-De-Castro, A.; Roncero-Sanchez, P.; Moreno-Munoz, A. Microgrids Power Quality Enhancement Using Model Predictive Control. *Electronics* **2021**, *10*, 328. [CrossRef]
11. Alshehri, J.; Khalid, M. Power Quality Improvement in Microgrids Under Critical Disturbances Using an Intelligent Decoupled Control Strategy Based on Battery Energy Storage System. *IEEE Access* **2019**, *7*, 147314–147326. [CrossRef]
12. Mosaad, M.I.; Ramadan, H. Power quality enhancement of grid-connected fuel cell using evolutionary computing techniques. *Int. J. Hydrog. Energy* **2018**, *43*, 11568–11582. [CrossRef]
13. Kaushal, J.; Basak, P. Power quality control based on voltage sag/swell, unbalancing, frequency, THD and power factor using artificial neural network in P.V. integrated A.C. microgrid. Sustain. *Energy Grids Netw.* **2020**, *23*, 100365.
14. Barik, P.K.; Shankar, G.; Sahoo, P.K. Power quality assessment of microgrid using fuzzy controller aided modified SRF based designed SAPF. *Int. Trans. Electr. Energy Syst.* **2019**, *30*, e12289. [CrossRef]
15. Esmaeili, M.; Shayeghi, H.; Valipour, K.; Safari, A.; Sedaghati, F. Power quality improvement of multi-microgrid using improved custom power device called as distributed power condition controller. *Int. Trans. Electr. Energy Syst.* **2020**, *30*, e12259. [CrossRef]
16. Salem, A.E.-S.; Salim, O.M.; Arafa, S.I. New triple-action controller for inverter power quality improvement. *Comput. Electr. Eng.* **2019**, *81*, 106543. [CrossRef]
17. Shahbaz, R.; Ahmed, T.; Elavarasan, R.M.; Raju, K.; Waqas, M.; Subramaniam, U. Selective Harmonics Elimination in Multilevel Inverter Using Bio-Inspired Intelligent Algorithms. In Proceedings of the 2021 31st Australasian Universities Power Engineering Conference (AUPEC), Perth, Australia, 26–30 September 2021. [CrossRef]
18. Haiya, Q.; Xu, Q.; Jun, Z.; Yuan, X. A robust GPS-based control scheme for power sharing and quality improvement in microgrid. *Int. J. Electr. Power Energy Syst.* **2020**, *123*, 106324.
19. Jahan, S.; Biswas, S.; Hosain, K.; Islam, R.; Haq, S.; Kouzani, A.; Mahmud, M. An Advanced Control Technique for Power Quality Improvement of Grid-Tied Multilevel Inverter. *Sustainability* **2021**, *13*, 505. [CrossRef]
20. Kenjrawy, H.; Makdisie, C.; Houssamo, I.; Mohammed, N. New Modulation Technique in Smart Grid Interfaced Multilevel UPQC-PV Controlled via Fuzzy Logic Controller. *Electronics* **2022**, *11*, 919. [CrossRef]
21. Peter, J.; Mohammed Shafi, K.P.; Lakshmi, R.; Ramchand, R. Nearly Constant Switching Space Vector Based Hysteresis Controller for VSI Fed IM Drive. *IEEE Trans. Ind. Appl.* **2018**, *54*, 3360–3371. [CrossRef]
22. Lin, X.; Huang, W.; Wang, L. SVPWM Strategy Based on the Hysteresis Controller of Zero-Sequence Current for Three-Phase Open-End Winding PMSM. *IEEE Trans. Power Electron.* **2018**, *34*, 3474–3486. [CrossRef]
23. Grady, W.M.; Mansoor, A.; Fuchs, E.F.; Verde, P.; Doyle, M. Estimating the net harmonic currents produced by selected distributed single-phase loads: Computers, televisions, and incandescent light dimmers. In Proceedings of the 2002 IEEE Power Engineering Society Winter Meeting, New York, NY, USA, 27–31 January 2002.
24. Yi, H.; Zhuo, F.; Wang, F.; Wang, Z. A Digital Hysteresis Current Controller for Three-Level Neural-Point-Clamped Inverter With Mixed-Levels and Prediction-Based Sampling. *IEEE Trans. Power Electron.* **2015**, *31*, 3945–3957. [CrossRef]
25. Buso, S.; Caldognetto, T. A Nonlinear Wide-Bandwidth Digital Current Controller for D.C.–D.C. and D.C.–A.C. *Convert. IEEE Trans. Ind. Electron.* **2015**, *62*, 7687–7695. [CrossRef]
26. Martins, D.C.; Casaro, M.M.; Barbi, I. Isolated three-phase rectifier with high power factor using the zeta converter in continuous conduction mode. *IEEE Trans. Circuits Syst. I Fundam. Theory Appl.* **2002**, *48*, 74–80. [CrossRef]
27. Wu, T.-F.; Liang, S.-A.; Chen, Y.-M.; Liang, S.-A. Design optimization for asymmetrical ZVS-PWM zeta converter. *IEEE Trans. Aerosp. Electron. Syst.* **2003**, *39*, 521–532. [CrossRef]
28. Lin, B.R.; Hsieh, F.Y. Soft-Switching Zeta–Flyback Converter With a Buck–Boost Type of Active Clamp. *IEEE Trans. Ind. Electron.* **2007**, *54*, 2813–2822.

29. Wang, D.; Ji, G.; Li, J.; Sun, H.; Liu, S.; Song, K. A novel hysteresis current control strategy based on neural network. In Proceedings of the 2010 International Conference On Computer Design and Application, Qinhuangdao, China, 25–27 June 2010; pp. V2-369–V2-372. [CrossRef]
30. Karabag, Y.; Erfidan, T.; Urgun, S.; Abut, N. Artificial neural network based hysteresis current controller for single-phase inverter. In Proceedings of the 12th IEEE Mediterranean Electrotechnical Conference (IEEE Cat. No.04CH37521), Dubrovnik, Croatia, 12–15 May 2004; Volume 1, pp. 339–341. [CrossRef]
31. Kumar, R.; Singh, B. BLDC Motor Driven Solar P.V. Array Fed Water Pumping System Employing Zeta Converter. *IEEE Trans. Ind. Appl.* **2016**, *52*, 2315–2322. [CrossRef]
32. Hmidet, A.; Subramaniam, U.; Elavarasan, R.M.; Raju, K.; Diaz, M.; Das, N.; Mehmood, K.; Karthick, A.; Muhibbullah, M.; Boubaker, O. Design of Efficient Off-Grid Solar Photovoltaic Water Pumping System Based on Improved Fractional Open Circuit Voltage MPPT Technique. *Int. J. Photoenergy* **2021**, *2021*, 1–18. [CrossRef]